

# Cavity-stabilized laser with acceleration sensitivity below $10^{-12} \text{ g}^{-1}$

David R. Leibrandt,<sup>\*</sup> James C. Bergquist, and Till Rosenband*National Institute of Standards and Technology, 325 Broadway Street, Boulder, Colorado 80305, USA*

(Received 31 December 2012; published 21 February 2013)

We characterize the frequency sensitivity of a cavity-stabilized laser to inertial forces and temperature fluctuations, and perform real-time feedforward to correct for these sources of noise. We measure the sensitivity of the cavity to linear accelerations, rotational accelerations, and rotational velocities by rotating it about three axes with accelerometers and gyroscopes positioned around the cavity. The worst-direction linear acceleration sensitivity of the cavity is  $2(1) \times 10^{-11} \text{ g}^{-1}$  measured over 0–50 Hz, which is reduced by a factor of 50 to below  $10^{-12} \text{ g}^{-1}$  for low-frequency accelerations by real-time feedforward corrections of all of the aforementioned inertial forces. A similar idea is demonstrated in which laser frequency drift due to temperature fluctuations is reduced by a factor of 70 via real-time feedforward from a temperature sensor located on the outer wall of the cavity vacuum chamber.

DOI: [10.1103/PhysRevA.87.023829](https://doi.org/10.1103/PhysRevA.87.023829)

PACS number(s): 42.62.Eh, 42.60.Da, 46.40.–f, 07.07.Tw

## I. INTRODUCTION

Frequency-stable lasers are indispensable tools for precision measurements, finding applications ranging from optical frequency standards [1–3] and tests of fundamental physics [4–6] to geodesy [7,8] and low-phase-noise microwave synthesis [9–12]. Typically, lasers for such applications are stabilized by locking them to a Fabry-Pérot cavity such that the fractional frequency stability of the laser is determined by the fractional length stability of the cavity [13–18]. Such cavity-stabilized lasers are sensitive to environmental perturbations that change the length of the cavity, including vibrations and temperature fluctuations, and much effort has gone into designing cavities that are less sensitive to accelerations [19–22] and shielding them from temperature fluctuations [23]. For applications outside the laboratory, such as clock-based geodesy [7,8], it is desirable to further reduce the sensitivity of laser frequencies to environmental perturbations.

A complementary approach to the passive reduction of the vibration sensitivity of cavity-stabilized lasers has been demonstrated [24,25] in which the acceleration environment is measured and real-time feedforward is applied to correct the frequency of the laser for the acceleration-induced frequency fluctuations. This approach also yields information about the transfer function that describes how accelerations change the length of the cavity, which can in turn be used to improve the cavity design to achieve a lower passive vibration sensitivity. In previous work, feedforward corrected for first-order deformations of the cavity due to linear and rotational accelerations over a bandwidth of 0.06–450 Hz. Here, we extend this approach to include feedforward that corrects for first- and second-order deformations of the cavity due to all of the (rigid body) inertial forces, namely rotational velocity as well as linear and rotational acceleration, with a bandwidth that extends to zero frequency (0–300 Hz). In addition, we implement feedforward to correct for temperature fluctuations of the cavity by use of a temperature sensor located on the cavity vacuum chamber. This extended feedforward is combined with a redesigned cavity mount that improves the

passive acceleration sensitivity of the cavity to be equal to the best reported value for a Fabry-Pérot cavity [22].

This paper proceeds as follows. Section II describes the experimental setup, including details of the cavity mount design and feedforward implementation. Measurements of the acceleration sensitivity of the cavity and the frequency stability of the laser in a laboratory environment are presented in Sec. III. Finally, Secs. IV and V evaluate the performance of inertial force and temperature feedforward, respectively.

## II. SETUP

A drawing of the mounted cavity is shown in Fig. 1(a). The cavity design is similar to that described in Ref. [21]. Briefly, the spacer is a 50-mm-diameter sphere made of Corning Ultra-Low Expansion (ULE) glass [26]. There is a 6-mm-diameter hole drilled along the optical axis and mirrors are optically contacted to 15.2-mm-diameter flats polished onto the ends. A 4-mm-diameter hole is drilled orthogonal to the optical axis for vacuum pumpout. The symmetry of the cavity geometry serves to reduce the acceleration sensitivity [19,21]. The 12.7-mm-diameter by 4-mm-thick mirrors are made of fused silica for reduced thermomechanical noise [27–29]. Both mirrors have a radius of curvature of 50 cm and the measured cavity finesse is  $7.9(8) \times 10^5$  at the operating wavelength of 1070 nm.

The cavity mount is improved over the one used in Ref. [21]. Stainless steel 304 flexure springs hold the cavity at two points on a diameter of the spherical spacer that is orthogonal to the optical axis. The springs are designed such that the rigid-body motional modes of the sphere within the mount are at frequencies of a few hundred hertz. This is a compromise between holding the sphere stiffly in order to maintain alignment of the laser to the cavity mode in the presence of  $2g$  acceleration changes, and holding the sphere weakly in order to reduce transmission of stresses due to vibrations and thermal expansion from the mount to the cavity ( $1g = 9.8 \text{ m/s}^2$ ). We calculate the frequencies of the rigid-body motional modes of the cavity using finite-element analysis to be at 280 Hz (translation along the mounting axis), 340 Hz (rotation about the mounting axis), 430 Hz (translation along the orthogonal axes), and 690 Hz (rotation about the orthogonal

---

<sup>\*</sup>david.leibrandt@nist.gov

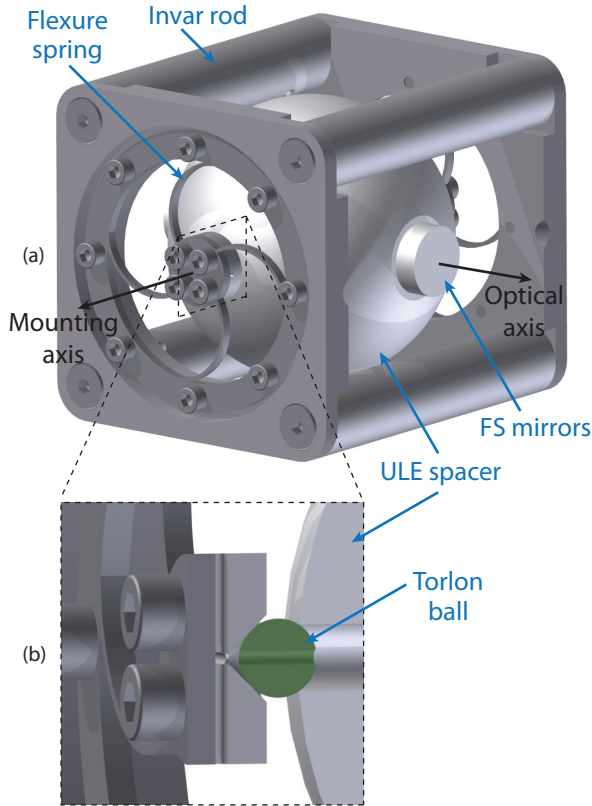


FIG. 1. (Color online) (a) Computer-aided design (CAD) drawing of the mounted Fabry-Pérot cavity. The spherical cavity spacer is 50 mm in diameter. (b) Cross-sectional view showing the details of the contact between the cavity and the mount. A Torlon ball is compressed between the flexure spring and the vacuum pump-out hole in the cavity. FS: fused silica.

axes). For reference, the lowest internal mechanical resonance of the spherical spacer is near 50 kHz.

Contact between the springs and the cavity spacer is made by two 4.8-mm-diameter vented Torlon [26] spheres that sit in the hole intended for vacuum evacuation [see Fig. 1(b)]. The Torlon spheres are held in place by a  $10^2$  N compressive preload of the springs. We find that the residual passive acceleration sensitivity depends primarily on stresses induced in the mounting structure during assembly. For example, we once disassembled and reassembled the cavity mount without (intentionally) making any changes and the linear acceleration sensitivity changed from  $1 \times 10^{-12} \text{ g}^{-1}$ ,  $35 \times 10^{-12} \text{ g}^{-1}$ , and  $55 \times 10^{-12} \text{ g}^{-1}$  to  $18 \times 10^{-12} \text{ g}^{-1}$ ,  $7 \times 10^{-12} \text{ g}^{-1}$ , and  $20 \times 10^{-12} \text{ g}^{-1}$  for accelerations along the optical axis, mounting axis, and an orthogonal axis, respectively. This suggests that in order to make further improvements to the passive acceleration sensitivity, it may be necessary to understand the contact forces between the cavity and the mounting structure in detail. Improvements may also be gained by use of a mounting structure that can be tuned to null the acceleration sensitivity *in situ* [22].

The cavity is held at a uniform and stable temperature by housing it in a thermal radiation shield inside a vacuum chamber. The vacuum chamber and radiation shield are made of aluminum (alloy 7075 for the vacuum chamber and 6061 for the radiation shield) with an electroless nickel coating, and

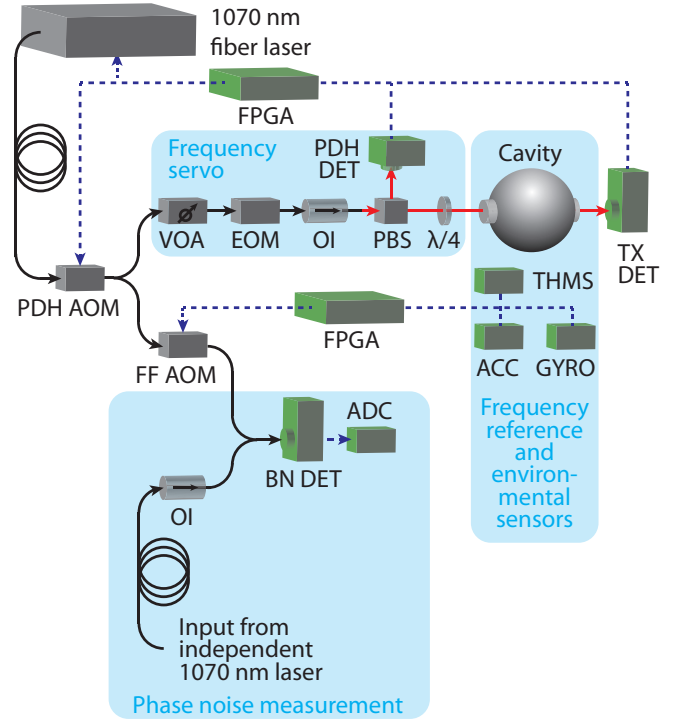


FIG. 2. (Color online) Schematic of the fiber-optic frequency servo and feedforward. A laser is stabilized to the length of a spherical Fabry-Pérot cavity by the PDH method. Environmental sensors detect inertial forces and temperature drift that perturb the length of the cavity; the resulting frequency perturbations of the laser are corrected by feedforward to the frequency of an AOM. The stability of the laser is measured by comparing it with an independent laser. Note that both the frequency servo and the feedforward are implemented entirely digitally in FPGAs. Black lines denote optical fiber, red lines denote free-space laser propagation, and blue dashed lines denote electrical signals. VOA: variable optical attenuator; OI: optical isolator; PBS: polarizing beam splitter;  $\lambda/4$ : quarter-wave plate; DET: detector; BN: beat note; TX: transmission; PDH: Pound-Drever-Hall; THMS: thermistor; ACC: accelerometer; GYRO: gyroscope. See text for other abbreviations.

conflat vacuum seals are made using aluminum gaskets [30]. This design takes advantage of the high thermal conductivity of aluminum and the low emissivity of nickel to ensure a uniform and stable temperature. The zero crossing of the cavity's coefficient of thermal expansion (CTE) is at approximately  $-17^\circ\text{C}$ , and we actively stabilize the temperature of the vacuum-chamber wall at  $24^\circ\text{C}$  by use of a thermoelectric cooler (TEC).

We lock a 1070 nm fiber laser to the cavity by the Pound-Drever-Hall (PDH) method [13] (see Fig. 2). To improve the long-term stability of the optical alignment, we employ primarily fiber-coupled optics such as a fiber-coupled waveguide electro-optic modulator (EOM) for phase modulation and fiber-coupled acousto-optic modulators (AOMs) [16] for closed-loop frequency feedback corrections and open-loop frequency feedforward corrections. There is roughly 3 m of optical fiber in the system, and it was not necessary to eliminate phase noise introduced by this optical fiber. The frequency servo is implemented digitally in a field-programmable gate array (FPGA) that feeds back to the frequency and amplitude

of an AOM, a piezoelectric transducer inside the laser, and the temperature of the laser. Typically, the laser stays locked for days at a time, and the laser optics were adjusted only once during the approximately one-year time period when data in this paper were collected.

We measure inertial forces and temperature drift, which perturb the length of the cavity, both to characterize the environmental sensitivity and to correct for the corresponding frequency perturbations of the laser via feedforward to the frequency of an AOM. Linear and rotational accelerations are measured by six one-axis variable-capacitance accelerometers (Dytran 7500A1 [26]) mounted around the cavity in a geometry where there is one sensor at the center of each face of a cube, with the sensing axis oriented on a diagonal of the cube face such that these diagonals form a regular tetrahedron [25,31]. The accelerometers have a  $-3$  dB bandwidth of 400 Hz. Rotational velocity is measured by three one-axis MEMS (microelectromechanical systems) gyroscopes (Analog Devices ADIS16130 [26]) with a  $-3$  dB bandwidth of 300 Hz. Simultaneously with the inertial forces, the temperature of the cavity is measured by a 5 k $\Omega$  thermistor mounted on the outside of the vacuum chamber. Feedforward is implemented digitally by use of a second FPGA which controls the frequency of an AOM.

The complete physics package, which includes the laser, cavity, frequency servo and feedforward optics, and environmental sensors, has a mass of 29 kg and dimensions of  $46 \times 46 \times 29$  cm<sup>3</sup>. For the broadband acceleration sensitivity measurements described in Sec. III, the package was mounted on a low-vibration shaker platform. For the low-frequency acceleration sensitivity measurements described in Sec. IV, the physics package was remounted in a structure similar to that of Ref. [22], which allowed the physics package to be rotated around three axes.

### III. FREQUENCY STABILITY AND CAVITY ACCELERATION SENSITIVITY

The frequency stability of the laser is measured via a heterodyne beat note with an independent reference laser that is located in another room. This reference laser typically serves as the clock laser that drives the  $^1S_0$  to  $^3P_0$  transition in  $^{27}\text{Al}^+$  [1,14], and is delivered to the experimental setup via a noise-canceled fiber [33]. Figures 3 and 4 show measurements of the laser frequency Allan deviation and power spectral density when the physics package is located on a passively isolated optical table. The Allan deviation of the laser frequency is  $2 \times 10^{-15}$  from 0.5 to 10 s both with and without applying the inertial force feedforward corrections (described in Sec. IV). The data show that the fractional frequency fluctuations are reduced by the application of the feedforward corrections for averaging times shorter than 0.5 s. Figure 3 indicates that accelerometer and gyroscope output noise are not a significant source of laser frequency noise. The frequency power spectral density shows several narrow spikes at harmonics of the laboratory electric-power frequency (60 Hz) as well as a couple of broader spikes near two of the calculated motional resonance frequencies of the cavity with respect to its mount (340 Hz and 690 Hz). These spikes do not contain a large

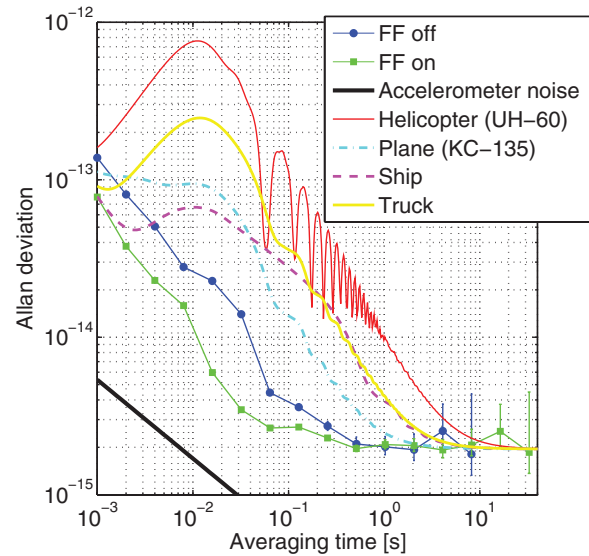


FIG. 3. (Color online) Allan deviation of the laser frequency when the physics package is located on a passively isolated optical table, with real-time inertial force feedforward (FF) off and on. The data with feedforward on is a 120 s data set with no drift removal. Also shown are the expected contribution of accelerometer noise to laser frequency noise and estimates of the laser stability if a vibration-insensitive laser were to be operated on several types of moving vehicles [32]. For these estimates, we assume the use of a hypothetical passive vibration isolation system that attenuates accelerations above 30 Hz by 40 dB per decade. To reach this performance, it will be necessary to extend the feedforward system, so that the low-frequency acceleration sensitivity of  $4 \times 10^{-13}$  g<sup>-1</sup> applies to the entire band of vehicle acceleration frequencies (0–2 kHz). The expected contribution of gyroscope noise to laser frequency noise,  $10^{-19}\tau^{-1}$ , where  $\tau$  is the averaging time in seconds, is not visible on this plot.

fraction of the laser power (both peaks together contain less than 3%).

The acceleration sensitivity of the cavity (without inertial force feedforward) is shown as a function of frequency over

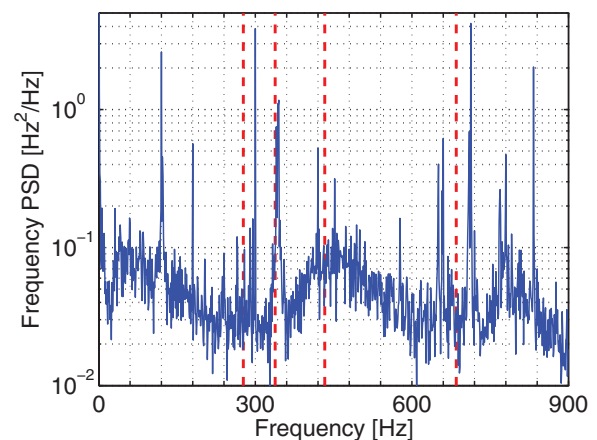


FIG. 4. (Color online) Laser frequency power spectral density with the physics package located on a passively isolated optical table, with real-time inertial force feedforward on. The resolution bandwidth is 1 Hz. Dashed lines denote the calculated frequencies of rigid-body motional resonances of the cavity within its mount.

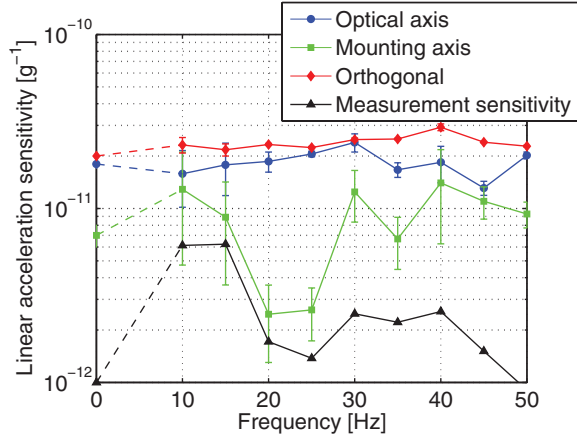


FIG. 5. (Color online) Linear acceleration sensitivity of the cavity versus frequency, without inertial force feedforward. These data were taken with the physics package sitting on a commercial active-vibration isolation (AVI) platform operated in reverse as a shaker. The measurement sensitivity shown in black is limited by the amplitude of vibrations that could be driven by the AVI platform. With the real-time inertial force feedforward on, the linear acceleration sensitivity was measured to be consistent with the measurement sensitivity over a frequency range of 0–30 Hz.

0–50 Hz in Fig. 5. This measurement is taken with the cavity on a platform that is actively shaken. The accelerations and resulting laser frequency noise are simultaneously recorded, and the results are Fourier-transformed and inverted to obtain the acceleration sensitivity for each direction as a function of frequency, as described in Ref. [21]. The acceleration sensitivity for accelerations along the most sensitive direction (an axis orthogonal to both the optical axis and the mounting axis) is  $2(1) \times 10^{-11} \text{ g}^{-1}$  over 0–50 Hz. We do not observe any unexpected mechanical resonances within the measured frequency range.

#### IV. INERTIAL FORCE FEEDFORWARD

Inertial force feedforward requires accurate knowledge of the transfer function that describes how linear accelerations,

rotational accelerations, and rotational velocities cause the length of the cavity’s optical axis to change. The inertial force sensitivity measurement described in Sec. III is limited to linear accelerations because our shaker platform cannot drive rotations. Furthermore, the signal-to-noise ratio of the measurement is low because the maximum amplitude of linear accelerations that can be applied is of the order of  $10^{-3} \text{ g}$ . In order to improve the accuracy of our knowledge of the transfer function, we remounted the physics package on a platform that allows rotation around three orthogonal axes [22]. This enables an accurate measurement of the transfer function for both rotational velocities and accelerations as well as linear accelerations (because the orientation of the cavity changes with respect to gravity), but only at very low frequencies.

First, we perform simultaneous measurements of the accelerometer and gyroscope outputs with the laser frequency while rotating the physics package by hand around three axes. We use these data to calculate the Wiener filter [24] with one tap for each of the following inputs along each axis: linear acceleration, linear acceleration squared, rotational acceleration, and rotational velocity squared. The discrete Laplace transform of these taps gives the first- and second-order passive sensitivity of the cavity length to low-frequency linear accelerations, rotational accelerations, and rotational velocity. The results are listed in the first group of three lines in Table I. Note that the second-order sensitivity to linear accelerations is a real effect; the accelerometers we use have a maximum specified nonlinearity of 0.25% at 1 g of acceleration, which is smaller than the measured second-order linear acceleration sensitivity. The measured inertial force transfer function is valid for the frequency range over which we can apply inertial forces by rotating the physics package, which is limited to below 1 Hz. We expect, however, that the inertial force transfer function is constant in frequency up to at least 50 Hz because we do not see any mechanical resonances in that frequency range (see Fig. 5).

After calibrating the Wiener filter taps we again rotate the physics package, while performing real-time inertial force feedforward. Simultaneously, we acquire a second set of measurements of the accelerometer and gyroscope outputs together with the laser frequency. From these data we obtain

TABLE I. Sensitivity of the laser frequency to slowly varying inertial forces. The origin of the coordinate system in which the inertial forces are measured is coincident with the center of the cavity. The first group of three lines are without real-time inertial force feedforward, the second group of three lines are with real-time feedforward, and the third group of three lines are with real-time feedforward, measured eight months later using the same Wiener filter taps. All values should be multiplied by  $10^{-12}$  to get the fractional frequency sensitivity. Units for  $\ddot{r}_i$ ,  $\ddot{\theta}_i$ , and  $\dot{\theta}_i$  are  $\text{m/s}^2$ ,  $\text{rad/s}^2$ , and  $\text{rad/s}$ . The acceleration due to gravity at the Earth’s surface,  $g$ , is equal to  $9.8 \text{ m/s}^2$ .

	Optical axis		Mounting axis		Orthogonal	
Linear acceleration	$+18(1)(\ddot{r}_x/g)$	$-1(1)(\ddot{r}_x/g)^2$	$-7(1)(\ddot{r}_y/g)$	$+2(1)(\ddot{r}_y/g)^2$	$+20(1)(\ddot{r}_z/g)$	$+3(1)(\ddot{r}_z/g)^2$
Rotational acceleration	$+0.04(2)\dot{\theta}_x$		$+0.10(2)\dot{\theta}_x$		$-0.10(2)\dot{\theta}_x$	
Rotational velocity		$+3.8(2)\dot{\theta}_x^2$		$-6.0(2)\dot{\theta}_y^2$		$-5.3(2)\dot{\theta}_z^2$
Linear acceleration	$+0(1)(\ddot{r}_x/g)$	$+1(1)(\ddot{r}_x/g)^2$	$+0(1)(\ddot{r}_y/g)$	$+0(1)(\ddot{r}_y/g)^2$	$+0(1)(\ddot{r}_z/g)$	$+0(1)(\ddot{r}_z/g)^2$
Rotational acceleration	$-0.01(2)\dot{\theta}_x$		$+0.03(2)\dot{\theta}_x$		$+0.00(2)\dot{\theta}_x$	
Rotational velocity		$+0.0(2)\dot{\theta}_x^2$		$+0.3(2)\dot{\theta}_y^2$		$+0.1(2)\dot{\theta}_z^2$
Linear acceleration	$+3(1)(\ddot{r}_x/g)$	$+0(1)(\ddot{r}_x/g)^2$	$+3(1)(\ddot{r}_y/g)$	$+2(1)(\ddot{r}_y/g)^2$	$+0(1)(\ddot{r}_z/g)$	$+3(1)(\ddot{r}_z/g)^2$
Rotational acceleration	$+0.02(2)\dot{\theta}_x$		$+0.00(2)\dot{\theta}_x$		$+0.02(2)\dot{\theta}_x$	
Rotational velocity		$-0.2(2)\dot{\theta}_x^2$		$+0.3(2)\dot{\theta}_y^2$		$+0.0(2)\dot{\theta}_z^2$

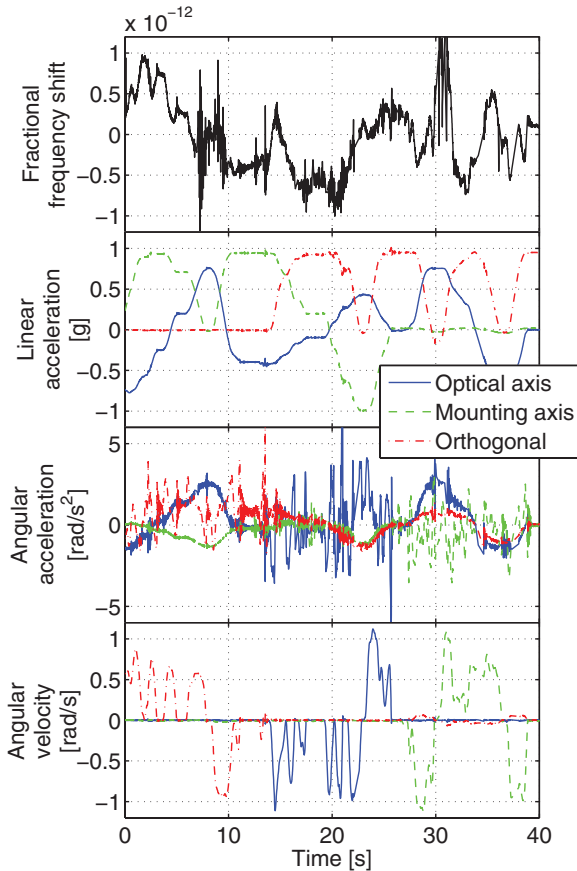


FIG. 6. (Color online) Fractional frequency shift of the output light versus time while rotating the laser and cavity about all three axes, with real-time inertial force feedforward on. Also shown from top to bottom are the linear acceleration, angular acceleration, and angular velocity experienced by the laser and cavity. The data are averaged in 10 ms bins. The root mean square (rms) fractional frequency noise of the laser is  $4.0 \times 10^{-13}$  and that of the feedforward corrections is  $2.0 \times 10^{-11}$ , so inertial force feedforward has reduced the laser frequency noise amplitude by a factor of 50 in this measurement. An estimate of the linear acceleration sensitivity with real-time inertial force feedforward can be obtained by dividing the rms fractional frequency noise by the rms acceleration (0.33, 0.47, and 0.73 g along the optical axis, mounting axis, and orthogonal axis) to obtain  $4 \times 10^{-13} \text{ g}^{-1}$ . The relative contributions of the different types of inertial forces to the feedforward frequency correction power are 96.8% first-order linear acceleration, 2.2% second-order linear acceleration, 0.1% first-order rotational acceleration, and 0.9% second-order rotational velocity.

the inertial force sensitivity of the laser frequency after real-time feedforward correction. The results, which are shown in the second group of three lines in Table I, are consistent with zero within our measurement sensitivity, which is  $10^{-12} \text{ g}^{-1}$  for linear accelerations. In other words, we are able to actively correct the inertial force sensitivity as well as we can measure it.

Figure 6 shows an example measurement of the inertial force sensitivity with real-time inertial force feedforward running, obtained by rotating the laser about three axes. In this data set, the laser frequency fluctuations due to inertial forces are reduced by a factor of 50 to a root mean square (rms) fractional amplitude of  $4.0 \times 10^{-13}$ . We can get an upper

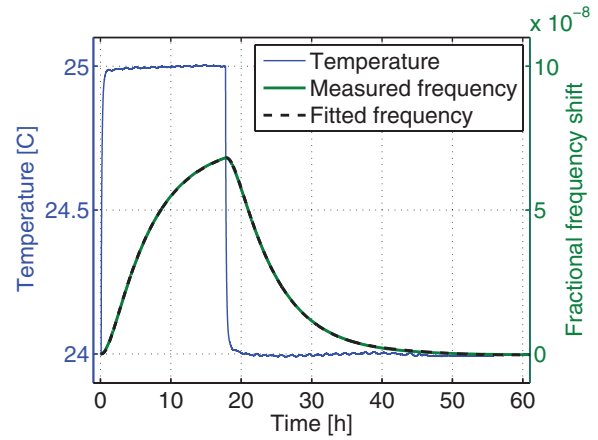


FIG. 7. (Color online) Fractional frequency shift of the laser (green line) while the temperature of the vacuum chamber which holds the cavity (blue line) is stepped by 1 K. The fit (black dashed line) is a second-order low-pass filter of the measured temperature with time constants of 1.1 and 6.1 h, scaled by  $7.3 \times 10^{-8} \text{ K}^{-1}$ .

bound of the first-order linear acceleration sensitivity from this data, assuming that the acceleration sensitivity is isotropic and that the accelerations applied along the three axes are linearly independent, by dividing the rms fractional frequency noise by the rms acceleration (0.33, 0.47, and 0.73 g along the optical axis, mounting axis, and orthogonal axis) to obtain  $4 \times 10^{-13} \text{ g}^{-1}$ . This is consistent with the values reported in the second group of three lines in Table I. Figure 3 includes an estimate of the laser frequency noise due to accelerations if a laser with an acceleration sensitivity of  $4 \times 10^{-13} \text{ g}^{-1}$  were to be operated in several varieties of moving vehicles.

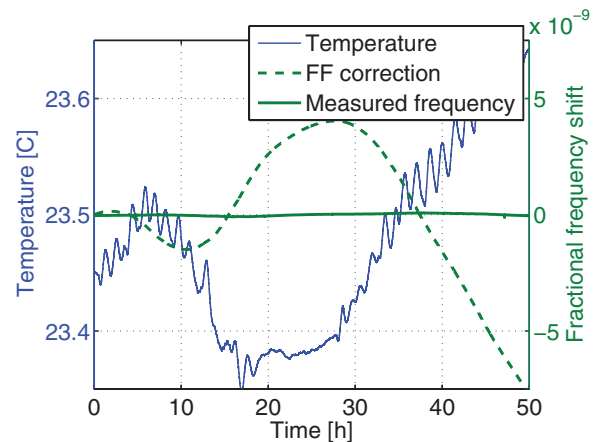


FIG. 8. (Color online) Temperature of the vacuum chamber that holds the cavity (blue line) and the corresponding fractional frequency shift of the laser (green line) while the temperature of the vacuum chamber is measured and thermal length changes of the cavity are compensated by feedforward to the frequency of an acousto-optic modulator (AOM). Temperature control of the vacuum chamber is disabled during this measurement, so the vacuum chamber temperature drifts with the temperature of the laboratory. The root mean square (rms) fractional frequency shift of the laser is  $4.5 \times 10^{-11}$  and that of the feedforward corrections is  $3.0 \times 10^{-9}$ , so temperature feedforward has reduced the laser frequency noise by a factor of 70 in this measurement.

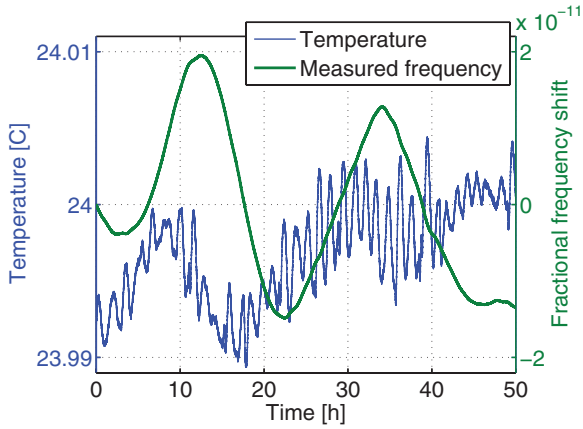


FIG. 9. (Color online) Temperature of the vacuum chamber that holds the cavity (blue line) and the corresponding fractional frequency shift of the laser (green line) while the temperature of the vacuum chamber is stabilized. The root mean square (rms) fractional frequency shift of the laser is  $1.0 \times 10^{-11}$ .

In order to investigate the long-term stability of the acceleration sensitivity, we remeasured the acceleration sensitivity eight months after the first measurement with real-time inertial force feedforward running using the same Wiener filter taps as the first measurement. The results are listed in the third group of three lines in Table I. The linear acceleration sensitivity changed by  $3 \times 10^{-12} \text{ g}^{-1}$  for accelerations along two directions. We have verified that this is due to a change of the passive acceleration sensitivity of the cavity, which may be caused by material creep of the cavity or mounting structure. Long-term operation of this system with an acceleration sensitivity below  $10^{-12} \text{ g}^{-1}$  would thus require periodic recalibration of the Wiener filter taps.

## V. TEMPERATURE FEEDFORWARD

We measure the transfer function from temperature fluctuations of the environment to length changes of the cavity by simultaneously recording the temperature of the vacuum chamber and the frequency of the laser while making a step in the set point of the vacuum-chamber temperature controller. The results are shown in Fig. 7. The measured laser frequency is fitted to a second-order low-pass filter of the measured temperature with time constants of 1.1 and 6.1 h, scaled by  $7.3 \times 10^{-8} \text{ K}^{-1}$ . We use this temperature sensitivity in a finite-element model of the cavity to determine that the zero crossing of the cavity's CTE is at approximately  $-17^\circ\text{C}$  [34,35]. The time constants are in reasonable agreement with estimates of the thermal conductivity between the vacuum chamber and the radiation shield and between the radiation shield and the cavity.

We implement real-time temperature feedforward using the transfer function measured above, discretized with a

1.1 s time step. Note that we position the temperature sensor on the outside of the vacuum chamber intentionally, rather than on the radiation shield or on the cavity itself, because in this configuration the sensor's noise is heavily low-pass filtered by the long radiative time constants before it is added onto the laser frequency. Figure 8 shows a measurement in which the temperature controller is disabled, and the cavity temperature drifts with the laboratory temperature. Real-time temperature feedforward reduces the laser frequency shift by a factor of 70, to a rms fractional frequency shift of  $4.5 \times 10^{-11}$  in an environment where the temperature of the vacuum chamber drifts by 80 mK rms. These residual frequency fluctuations can be compared with the rms fractional frequency shift with the temperature controller enabled shown in Fig. 9, which is  $1.0 \times 10^{-11}$ . While the performance of temperature feedforward is worse than temperature control (i.e., feedback) in this implementation, this trade-off might be acceptable for some applications where power is limited (e.g., field [21] or cryogenic [16,36] systems). Temperature feedforward might also be improved by using multiple or more precise temperature sensors.

## VI. CONCLUSION

We have demonstrated, by a combination of an improved cavity-mount design and real-time feedforward that corrects for all of the inertial forces to second-order, a cavity-stabilized laser with acceleration sensitivity below  $10^{-12} \text{ g}^{-1}$ . The performance of inertial force feedforward in this work is limited, at least in part, by our inability to measure the transfer function with sufficient accuracy. It may be possible to obtain more complete knowledge of the transfer function, and thus better feedforward reduction of the acceleration sensitivity, with the use of a shaker table capable of applying broadband, six degree-of-freedom, large-amplitude accelerations. In addition, we have shown that feedforward can also be used to reduce laser frequency noise due to temperature fluctuations by use of a temperature sensor located on the outside of the vacuum chamber. These two examples illustrate the power and generality of feedforward for laser frequency stabilization: laser frequency noise caused by environmental fluctuations can be strongly reduced, as long as the environmental variable can be precisely measured and the transfer function accurately known.

## ACKNOWLEDGMENTS

We thank R. Drullinger, M. Notcutt, and M. Thorpe for their contributions to earlier work on low acceleration sensitivity lasers and also for useful discussions, R. Lalezari for fabrication of the cavity used in this work, and A. Ludlow and W. Swann for critical readings of this manuscript. This work is supported by AFOSR, DARPA QuASAR, and ONR and is not subject to US copyright.

- [1] C. W. Chou, D. B. Hume, J. C. J. Koelemeij, D. J. Wineland, and T. Rosenband, *Phys. Rev. Lett.* **104**, 070802 (2010).  
 [2] N. Huntemann, M. Okhapkin, B. Lipphardt, S. Weyers, C. Tamm, and E. Peik, *Phys. Rev. Lett.* **108**, 090801 (2012).

- [3] A. A. Madej, P. Dubé, Z. Zhou, J. E. Bernard, and M. Gertsvolf, *Phys. Rev. Lett.* **109**, 203002 (2012).  
 [4] T. Rosenband, D. B. Hume, P. O. Schmidt, C. W. Chou, A. Brusch, L. Lorini, W. H. Oskay, R. E. Drullinger,

- T. M. Fortier, J. E. Stalnaker *et al.*, *Science* **319**, 1808 (2008).
- [5] C. Eisele, A. Y. Nevsky, and S. Schiller, *Phys. Rev. Lett.* **103**, 090401 (2009).
- [6] S. Reynaud, C. Salomon, and P. Wolf, *Space Sci. Rev.* **148**, 233 (2009).
- [7] C. W. Chou, D. B. Hume, T. Rosenband, and D. J. Wineland, *Science* **329**, 1630 (2010).
- [8] R. Bondarescu, M. Bondarescu, G. Hetényi, L. Boschi, P. Jetzer, and J. Balakrishna, *Geophys. J. Int.* **191**, 78 (2012).
- [9] E. Baumann, F. R. Giorgetta, J. W. Nicholson, W. C. Swann, I. Coddington, and N. R. Newbury, *Opt. Lett.* **34**, 638 (2009).
- [10] W. Zhang, Z. Xu, M. Lours, R. Boudot, Y. Kersale, G. Santarelli, and Y. Le Coq, *Appl. Phys. Lett.* **96**, 211105 (2010).
- [11] T. M. Fortier, M. S. Kirchner, F. Quinlan, J. Taylor, J. C. Bergquist, T. Rosenband, N. Lemke, A. Ludlow, Y. Jiang, C. W. Oates *et al.*, *Nat. Photonics* **5**, 425 (2011).
- [12] A. J. Benedick, J. G. Fujimoto, and F. X. Kärtner, *Nat. Photonics* **6**, 97 (2012).
- [13] R. W. P. Drever, J. L. Hall, F. V. Kowalski, J. Hough, G. M. Ford, A. J. Munley, and H. Ward, *Appl. Phys. B* **31**, 97 (1983).
- [14] B. C. Young, F. C. Cruz, W. M. Itano, and J. C. Bergquist, *Phys. Rev. Lett.* **82**, 3799 (1999).
- [15] Y. Y. Jiang, A. D. Ludlow, N. D. Lemke, R. W. Fox, J. A. Sherman, L.-S. Ma, and C. W. Oates, *Nat. Photonics* **5**, 158 (2011).
- [16] T. Kessler, C. Hagemann, C. Grebing, T. Legero, U. Sterr, F. Riehle, M. J. Martin, L. Chen, and J. Ye, *Nat. Photonics* **6**, 687 (2012).
- [17] Q.-F. Chen, A. Nevsky, and S. Schiller, *Appl. Phys. B* **107**, 679 (2012).
- [18] T. L. Nicholson, M. J. Martin, J. R. Williams, B. J. Bloom, M. Bishof, M. D. Swallows, S. L. Campbell, and J. Ye, *Phys. Rev. Lett.* **109**, 230801 (2012).
- [19] M. Notcutt, L.-S. Ma, J. Ye, and J. L. Hall, *Opt. Lett.* **30**, 1815 (2005).
- [20] J. Millo, D. V. Magalhães, C. Mandache, Y. Le Coq, E. M. L. English, P. G. Westergaard, J. Lodewyck, S. Bize, P. Lemonde, and G. Santarelli, *Phys. Rev. A* **79**, 053829 (2009).
- [21] D. R. Leibrandt, M. J. Thorpe, M. Notcutt, R. E. Drullinger, T. Rosenband, and J. C. Bergquist, *Opt. Express* **19**, 3471 (2011).
- [22] S. Webster and P. Gill, *Opt. Lett.* **36**, 3572 (2011).
- [23] S. T. Dawkins, R. Chicireanu, M. Petersen, J. Millo, D. V. Magalhães, C. Mandache, Y. Le Coq, and S. Bize, *Appl. Phys. B* **99**, 41 (2010).
- [24] M. J. Thorpe, D. R. Leibrandt, T. M. Fortier, and T. Rosenband, *Opt. Express* **18**, 18744 (2010).
- [25] D. R. Leibrandt, M. J. Thorpe, J. C. Bergquist, and T. Rosenband, *Opt. Express* **19**, 10278 (2011).
- [26] Commercial products are identified for technical clarity. Such identification does not imply endorsement by the National Institute of Standards and Technology.
- [27] K. Numata, A. Kemery, and J. Camp, *Phys. Rev. Lett.* **93**, 250602 (2004).
- [28] M. Notcutt, L.-S. Ma, A. D. Ludlow, S. M. Foreman, J. Ye, and J. L. Hall, *Phys. Rev. A* **73**, 031804 (2006).
- [29] T. Kessler, T. Legero, and U. Sterr, *J. Opt. Soc. Am. B* **29**, 178 (2012).
- [30] F. Watanabe, Y. Koyatsu, K. Fujimori, H. Miki, A. Kasai, T. Sato, and K. Miyamoto, *J. Vac. Sci. Technol. A* **13**, 140 (1995).
- [31] J.-H. Chen, S.-C. Lee, and D. B. DeBra, *J. Guid. Control Dyn.* **17**, 286 (1994).
- [32] Department of Defense, *MIL-STD-810G, Environmental Engineering Considerations and Laboratory Tests* (2008).
- [33] L. S. Ma, P. Jungner, J. Ye, and J. L. Hall, *Opt. Lett.* **19**, 1777 (1994).
- [34] R. W. Fox, *Opt. Express* **17**, 15023 (2009).
- [35] T. Legero, T. Kessler, and U. Sterr, *J. Opt. Soc. Am. B* **27**, 914 (2010).
- [36] M. J. Thorpe, L. Rippe, T. M. Fortier, M. S. Kirchner, and T. Rosenband, *Nat. Photonics* **5**, 688 (2011).